MATERIALS

10.1126/sciadv.1500857

Carbyne with finite length: The one-dimensional *sp* carbon

Bitao Pan,* Jun Xiao,* Jiling Li,* Pu Liu, Chengxin Wang, Guowei Yang†

Carbyne is the one-dimensional allotrope of carbon composed of *sp*-hybridized carbon atoms. Definitive evidence for carbyne has remained elusive despite its synthesis and preparation in the laboratory. Given the remarkable technological breakthroughs offered by other allotropes of carbon, including diamond, graphite, fullerenes, carbon nanotubes, and graphene, interest in carbyne and its unusual potential properties remains intense. We report the first synthesis of carbyne with finite length, which is clearly composed of alternating single bonds and triple bonds, using a novel process involving laser ablation in liquid. Spectroscopic analyses confirm that the product is the structure of *sp* hybridization with alternating carbon-carbon single bonds and triple bonds and capped by hydrogen. We observe purple-blue fluorescence emissions from the gap between the highest occupied molecular orbital and the lowest unoccupied molecular orbital of carbyne. Condensed-phase carbyne crystals have a hexagonal lattice and resemble the white crystalline powder produced by drying a carbyne solution. We also establish that the combination of gold and alcohol is crucial to carbyne formation because carbon-hydrogen bonds can be cleaved with the help of gold catalysts under the favorable thermodynamic environment provided by laser ablation in liquid and because the unique configuration of two carbon atoms in an alcohol molecule matches the elementary entity of carbyne. This laboratory synthesis of carbyne will enable the exploration of its properties and applications.

INTRODUCTION

The discovery of fullerene in 1985 initiated exciting new research on allotropes of carbon, including carbon nanotubes and, more recently, graphene; significant scientific discoveries and technological advances have been made based on these new carbon materials (*1*, *2*). The well-established forms of carbon are diamond (with three-dimensional sp^3-hybridized carbon atoms) and graphite (with two-dimensional sp^2-hybridized carbon atoms), which have been known and used for millennia (*3*). More carbon allotropes have been discovered, such as fullerenes (*1*), nanotubes (*4*), and graphene (consisting of sp^2-hybridized carbon atoms), and lonsdaleite (*5*) and C_8 (*6*) (composed of sp^3-hybridized carbon atoms); each shows unusual properties, which are usually different from those of either diamond or graphite, offering technological breakthroughs (*2*). A third type of carbon atom hybridization, namely, one-dimensional *sp* hybridization, gives the allotrope carbyne, a one-dimensional form of carbon consisting of *sp*-hybridized carbon atoms; diamond and graphite are three-dimensional and two-dimensional forms of carbon, respectively (Fig. 1).

Carbyne is elusive and has so far proved impossible to synthesize in a well-defined form in the laboratory (*7*, *8*). Astrophysicists have proposed that, based on the observation of a new hexagonal carbon phase in meteorites, carbyne might exist as meteorites (*9*) and as a by-product of shock-fused graphite (*10*). Materials physicists have reported the presence of similar hexagonal carbon phases in the laboratory syntheses of carbyne by a number of routes, such as graphite sublimation and dehydrohalogenation of polymers (*11*, *12*). In these cases, there was no substantial evidence of the existence of carbyne (that is, a linear one-dimensional framework composed of *sp*-hybridized carbon atoms) in the resulting products. Synthetic chemists have therefore synthesized series of conjugated polyynes as carbyne models (*13*, *14*). However, carbyne crystals (the condensed phase of carbyne), which are proposed to have a hexagonal phase constructed of one-dimensional carbyne (*15*), have not been obtained by synthetic chemists. On all accounts, the resulting products or materials are ill-defined; definitive evidence for the existence of carbyne has not been obtained, and its specific properties have not yet been determined. Is carbyne a myth (*16*, *17*)?

Here, we show for the first time that carbyne with finite length can be synthesized under ambient conditions in the laboratory using a novel laser ablation in liquid (LAL) process (*18*) (the LAL process is shown in Supplementary Section I and fig. S1). We systemically and experimentally characterized this carbyne as follows. We show the first entire Raman spectrum of carbyne; it has two sharp peaks, at 1050 and 2175 cm^{-1}, characteristic of carbon-carbon single bonds and triple bonds, respectively. We also observed, for the first time, strong purple-blue fluorescence from the intrinsic emissions of carbyne. In addition, we produced hexagonal carbyne crystals as white powder (white carbon) from a solution of the synthesized carbyne. We established that the combination of gold and alcohol is crucial to carbyne formation in this case because carbon-hydrogen bonds can be cleaved with the help of gold catalysts under the favorable thermodynamic environment provided by LAL and because the unique configuration of two carbon atoms in an alcohol molecule matches the elementary entity of carbyne. These results show that researchers have synthesized the well-defined products of carbyne, implying that we are at the threshold of a new era of carbyne science and technology.

RESULTS

Carbyne synthesis was divided into two processes. First, a solution of the products was synthesized using LAL, and this solution was then purified using high-performance liquid chromatography (HPLC). The

State Key Laboratory of Optoelectronic Materials and Technologies, Nanotechnology Research Center, School of Physics and Engineering, Sun Yat-sen University, Guangzhou 510275, Guangdong, P. R. China.
*These authors contributed equally to this work.
†Corresponding author. E-mail: stsygw@mail.sysu.edu.cn

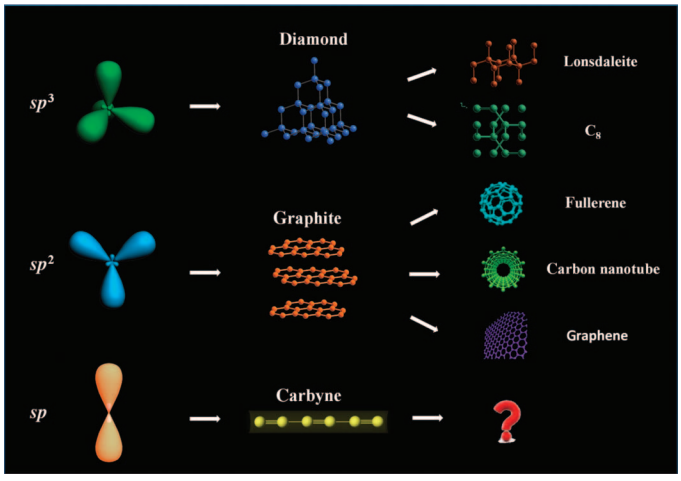

Fig. 1. Schematic illustration of the three kinds of hybridization of carbon. Diamond represents sp^3 hybridization, and its derivatives are lonsdaleite and C_8. The most familiar carbon material, graphite, shows sp^2 hybridization, and its derivatives are fullerene, carbon nanotube, and graphene. Carbyne is the one-dimensional allotrope of carbon composed of *sp*-hybridized carbon atoms. However, definitive evidence for carbyne remains elusive. Therefore, the existence of carbyne derivatives remains unknown.

samples obtained at a retention time of 2.3 min were collected for characterization. Raman spectroscopy is one of the techniques used to study carbon-based materials and to identify carbyne. The presence of a Raman band at about 2100 cm^{-1}, generated by carbon-carbon triple bonds, is strong evidence for the presence of carbines (*19*, *20*). The Raman signal of carbon-carbon single bonds is observed at about 1060 cm^{-1} (*21*). In our study, the micro-Raman spectra (633-nm laser source) of the samples showed two sharp peaks, at 1050 and 2175 cm^{-1}, which have been identified as the characteristic peaks of the carbon-carbon single bonds and triple bonds, respectively, of carbyne (Fig. 2A). A laser source with a different wavelength (514 nm) was also used for micro-Raman measurements (results shown in fig. S2). No other peaks were observed in the region 1000 to 3000 cm^{-1}. The full widths at half maximum values of the Raman peaks were small, suggesting that the sample has high purity and crystallinity. This was the first time that the Raman peak of carbyne carbon-carbon single bonds (at 1050 cm^{-1}) was observed.

The experimental measurements were verified by first-principles simulation of the Raman spectrum of carbyne with a chain of 10 carbon atoms (fig. S3). The theoretical calculation results were in agreement with the experimental data. The Raman spectra of the samples obtained at other HPLC retention times (such as 4.5 min) showed the signals for amorphous carbon and sp^2 carbon (fig. S4A). The carbon-carbon triple bonds of carbyne are commonly identified using Fourier transform infrared (FTIR) spectroscopy (*19*) The signal in the FTIR spectrum at 2157 cm^{-1} (Fig. 2B) was in agreement with the reported value for carbon-carbon triple bonds (between 2000 and 2200 cm^{-1}) (*19*). These spectroscopic analyses showed that carbyne with one-dimensional *sp* hybridization, consisting of alternating single bonds and triple bonds, was synthesized in our study.

The ultraviolet-visible (UV-Vis) absorption spectrum of the sample obtained at an HPLC retention time of 2.3 min is shown in Fig. 3A and fig. S5A. The peaks located at 230 and 238 nm were attributed to $\pi \rightarrow \pi^*$ absorption (*22*). The as-synthesized product and the sample

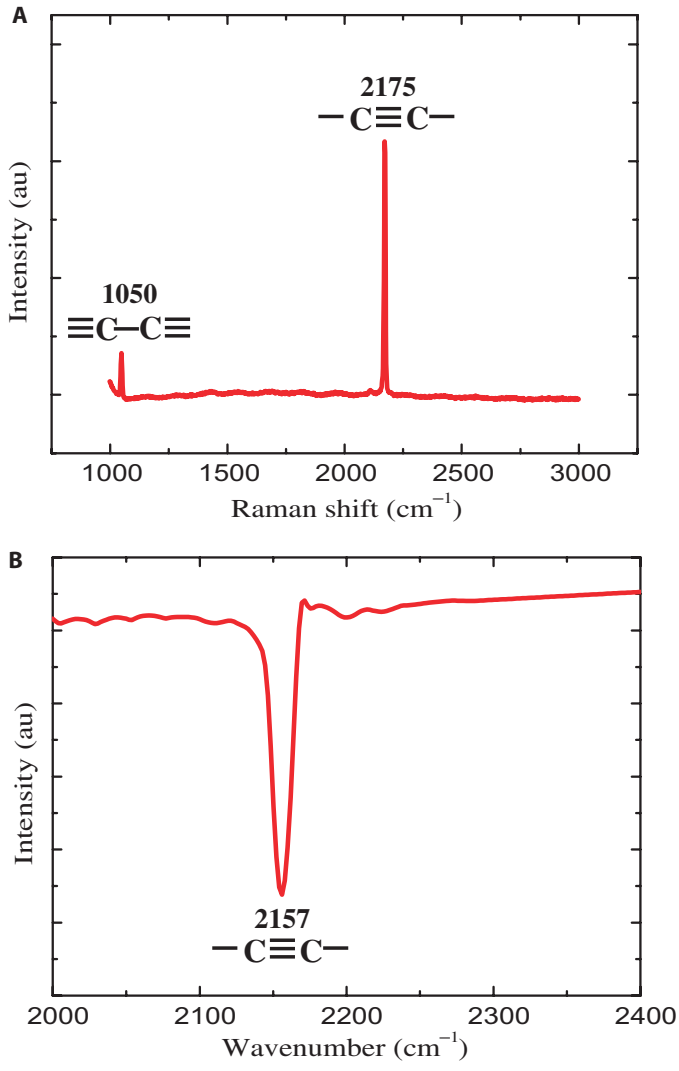

Fig. 2. Spectroscopic analysis of carbyne. (**A**) Raman spectrum. The peaks at 1050 and 2175 cm^{-1} belong to carbon-carbon single bonds and triple bonds, respectively. (**B**) FTIR spectrum. The signal at 2157 cm^{-1} is ascribed to the stretching vibration of carbon-carbon triple bonds.

obtained at 2.3 min via HPLC were transparent and colorless (Fig. 3A, inset). The UV-Vis spectrum of the as-synthesized products is shown in fig. S5B. The absorption peaks (230 and 238 nm) of the sample obtained at 2.3 min were stronger than those obtained before HPLC treatment. These two peaks were similar to the results of a hydrogen-terminated carbon chain with eight atoms (*23*). The corresponding mass spectrum and nuclear magnetic resonance (NMR) spectrum matched the carbon chain with *sp* hybridization well (detailed analysis in fig. S6). Strong purple-blue fluorescence was observed from a solution of the synthesized carbyne upon excitation from 330 to 400 nm at increments of 10 nm (Fig. 3B). Clearly, the fluorescence peaks at 410, 435, and 465 nm did not change with changing excitation wavelength, indicating that these peaks originated from an intrinsic carbyne emission. Purple-blue fluorescence (Fig. 3B, inset) can be observed with the naked eye upon irradiation with a 370-nm UV light. The decay time for carbyne was about 1.3 ns. No photobleaching of this sample was detected even after 1.5 hours of continuous excitation with a 450-W

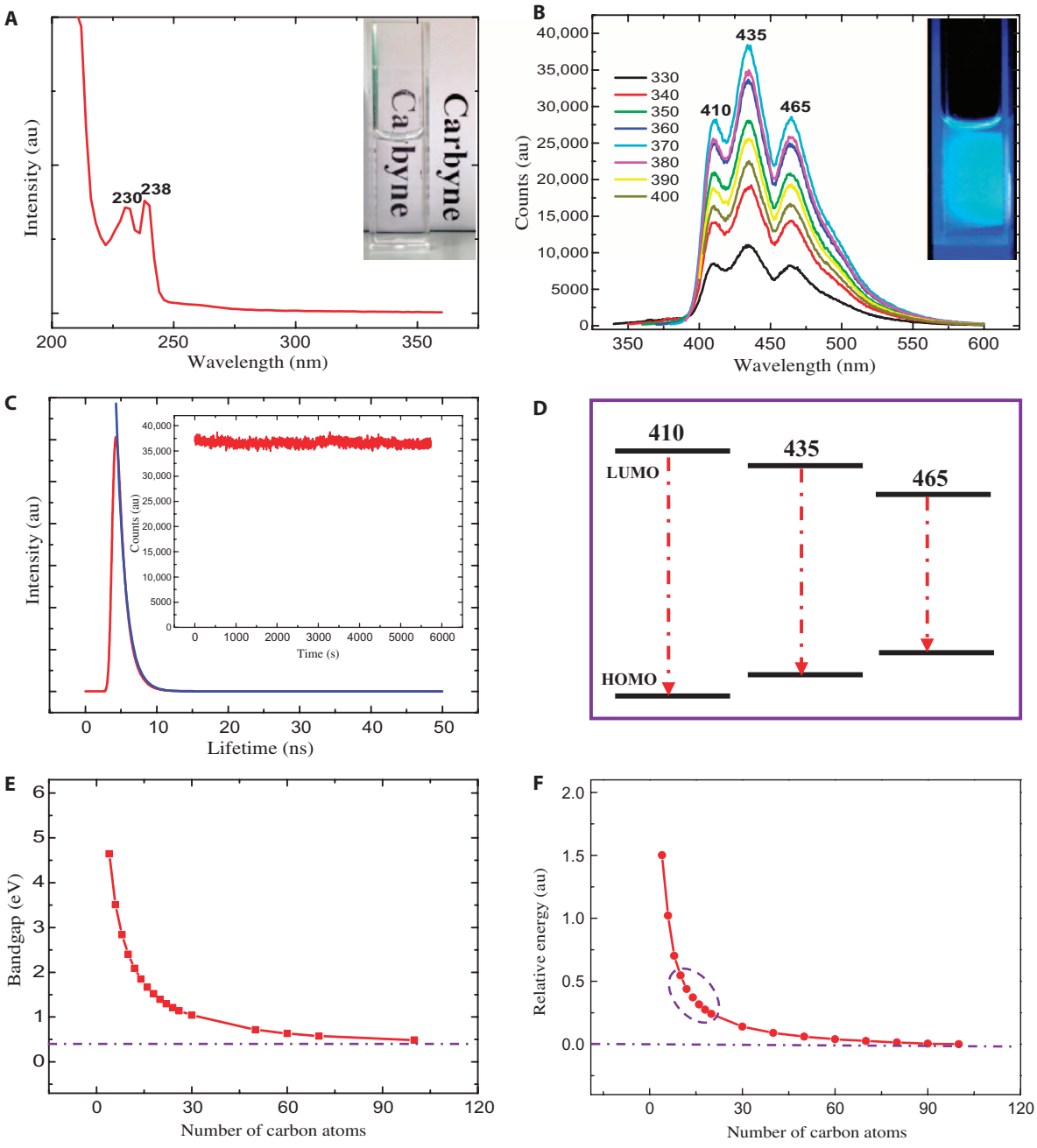

Fig. 3. UV-Vis and fluorescence spectra of carbyne. (**A**) UV-Vis absorption spectrum of the sample obtained at 2.3 min through HPLC (CH_3OH/H_2O; 97:3, v/v) and the corresponding optical graph of a colorless transparent solution. (**B**) Fluorescence emission of carbyne. Three fluorescence peaks (at 410, 435, and 465 nm) remain the same as excitation wavelength varies. Inset: The purple-blue fluorescence graph excited with a 370-nm light. (**C**) The lifetime of the sample is measured to be 1.3 ns. Inset: No photobleaching was observed with a 450-W xenon lamp across 1.5 hours. (**D**) Schematic illustration of three kinds of fluorescence behavior derived from different lengths of carbyne chains. (**E**) Dependence of energy gaps (ΔE) on the number of carbon atoms in carbyne. It is clear that the gaps between the highest occupied molecular orbital (HOMO) and the lowest unoccupied molecular orbital (LUMO) of carbyne monotonically decrease with increasing number of carbon atoms. For the 4- and 100-carbon carbynes, the HOMO-LUMO gap is 4.061 and 0.487 eV, respectively, implying the tuning of energy gaps (from broad to narrow) accompanying the increase in carbon atoms in carbyne. (**F**) For comparison, the relative energy in vertical coordinates represents the absolute value of relative binding energy. Negative binding energy corresponds to a stable configuration. The greater is the absolute value, the higher is the stability of carbyne chains. The relative absolute value of binding energy decreases with increasing number of carbon atoms in carbyne, but the decreasing speed gradually becomes slower and ultimately reaches a specific value. Dotted horizontal curve, trend reaching a specific value; circle, turning point in the curve.

xenon lamp (Fig. 3C, inset). However, the samples obtained at other HPLC retention times (such as 4.5 min) were not fluorescent (fig. S4B). This phenomenon is in agreement with the Raman results (that is, the samples obtained at other retention times were not carbyne). To the best of our knowledge, this is the first time that fluorescence emission from carbyne was observed.

Nanostructures synthesized using LAL (*18*) usually come in a range of sizes. The synthesized carbyne should therefore have a range of chain lengths. On the basis of our theoretical calculations (Fig. 3E), the gap between the highest occupied molecular orbital and the lowest unoccupied molecular orbital of carbyne changes with chain length, and there is a distinct trend toward a finite gap, estimated to be about 0.48 eV. Obviously, the bandgap of carbyne is determined by the corresponding chain length. Accordingly, the three fluorescence peaks, at 410, 435, and 465 nm, are probably derived from carbyne with 8 to 12 carbon atoms (Fig. 3D). To find out why these special carbynes are dominant in the sample, we calculated the stability of carbyne with different lengths. Figure 3F shows that the absolute values of relative binding energy decrease with an increasing number of carbon atoms in the carbyne. However, the decreasing speed gradually becomes slower and ultimately reaches a specific value. In other words, chains are inclined to grow longer as more energy is obtained. Thus, the thermodynamic force provided by LAL should drive carbyne to grow longer. A zone appears near 10 atoms (Fig. 3F), which seems to be "a dividing region" (dotted circle) in the curve indicating that binding energy dramatically changes with less than 10 atoms but only slightly changes with more than 10 atoms. Thus, this monotonic decline curve shows that the longer the chain is, the smaller the absolute value of the binding energy and the less stable it is; that is, carbyne driven by LAL tends to grow longer, but longer chains seem to be unstable. Thus, there must be a balance between them. In our case, LAL can supply the finite thermodynamic force needed to drive carbyne to form the chains with about 10 atoms, but it cannot promote longer chains with smaller absolute values of binding energy because of energy barrier.

We produced carbyne crystals by repeatedly dropping a carbyne solution onto silicon substrates and obtained white powders on substrate surfaces. The x-ray diffraction (XRD) pattern (Fig. 4A) shows clean, shaped, strong peaks, indicating carbyne crystals with good crystallinity. These peaks are indexed to the hexagonal structure of carbyne. Clearly, these white powders (that is, carbyne crystals) are polycrystalline. There is an obvious preferred orientation along the *c* axis. When these white powders were coated on glass substrates, the condensed phase of carbyne ("white carbon") (*10*, *11*) was obtained (Fig. 4A, inset). The scanning electron microscopy (SEM) image in Fig. 4B shows that the carbyne crystals consist of stacked flakes. In general, flake-like crystals readily grow along the *c* axis, consistent with the XRD pattern. The corresponding energy-dispersive x-ray spectrum (EDS) (Fig. 4B, inset) shows that the sample contains carbon, oxygen, and gold. The oxygen originates from surface adsorption. The corresponding transmission electron microscopy (TEM) image in Fig. 4C shows carbyne nanorods 10 to 30 nm wide and 50 to >100 nm long. The different morphologies observed in the TEM and SEM images are ascribed to different types of crystallization from the carbyne solution. The tiny spherical particles on the surfaces of carbyne nanorods are gold; this is why a gold signal is detected in the EDS for both SEM (Fig. 4B, inset) and TEM (Fig. 4J). The corresponding EDS for TEM shows that the sample is almost completely composed of carbon (95.6%). In addition, oxygen (2.42%) and copper (0.76%) peaks come from adsorbed oxygen molecules and the copper grid. A SiO film supported by formvar has also been used to confirm the origin of carbon and oxygen to more accurately check the element (fig. S7). Energy-dispersive x-ray (EDX) results obviously show that carbon content increased by 28% compared with that of the pure SiO film supported by formvar, indicating that carbyne is almost entirely made up of carbon (for a detailed analysis, see fig. S7). The corresponding selected area electron diffraction (SAED) patterns and high-resolution TEM (HRTEM) images of the carbyne crystals were obtained. We studied more than 30 carbyne crystals and divided their SAED patterns and HRTEM images into three categories based on the direction of the incident electron beam (that is, [1-20], [012], and [001]), as shown in Fig. 4 (D to I). Two of these are rectangular lattices, and one is a hexagonal lattice. A combination of these results and the XRD patterns shows that the carbyne crystal has a hexagonal structure with a = 5.78 Å, b = 5.78 Å, c = 9.10 Å, $\alpha = 90°$, $\beta = 90°$, and $\gamma = 120°$.

To clarify the crystalline structure of these carbyne crystals, we constructed the carbyne crystal structure shown in Fig. 5A based on three considerations. First, the Raman and FTIR spectra show that carbyne only contains *sp* hybridization; therefore, it is a one-dimensional chain. Second, the XRD and SAED patterns confirm a hexagonal structure; therefore, they can be used to directly determine the *a* and *b* lattice parameters in the *x-y* plane. Third, the length of *c* is obtained from the XRD pattern (that is, 9.1 Å). If the carbyne chain is straight (without kinks), the length of *c* should be the sum of the lengths of the carbon-carbon single bonds and triple bonds (about 2.6 Å); however, this does not match our experimental results. To resolve this dilemma, we used a kinked chain conformation (*15*). The lengths of the *c* axes are functions of the number of carbon atoms *n* in the chain and the kink angle (the angle between the vertical direction and the kinked bond). If we use eight carbon atoms in the chain and a kink angle of 30°, the *a* and *b* lattice parameters will be the same as the experimental value (5.78 Å) and the length of *c* will be 9.92 Å, which is the sum of the lengths of four carbon-carbon triple bonds and two carbon-carbon single bonds, plus two kinked bonds. The length was slightly longer than the experimental value (9.1 Å) because the lengths of the carbon-carbon single bond (1.33 Å) and triple bond (1.24 Å) were obtained from the carbyne chain after structure optimization. However, bending of the chain caused variations in bond length, leading to changes in chain length (*24*). We took these three factors into account in building the structural framework of the carbyne crystal (Fig. 5A). We found that the distance between neighboring carbon atoms was 3.34 Å, which is close to the layer spacing of graphite. The force connecting the carbon chains can therefore be considered as van der Waals forces. These characteristics exactly fit Heimann *et al.*'s (*15*) description of linear carbon polytypes, in which the chains are thought to be arranged parallel to the *c* axes and bonding is achieved by intermolecular linkages. Our constructed structural framework is therefore reasonable. To determine whether this proposed structure is stable, we calculated its stability using the SIESTA code (*25*), which is based on the standard Kohn-Sham self-consistent density functional theory. The equilibrium configuration obtained after structure optimization indicates that the proposed hexagonal model is stable (Fig. 5B). The kinked carbyne chains are unexpectedly deformed into a helix in the crystalline structure; therefore, the carbyne crystal resembles parallel arrays of helices. This helix-like shape is similar to the bent carbyne chains identified in the theoretical results (*24*). The carbyne chain can be easily bent with a small arc, and the thinnest carbon wire (an *sp*-carbon

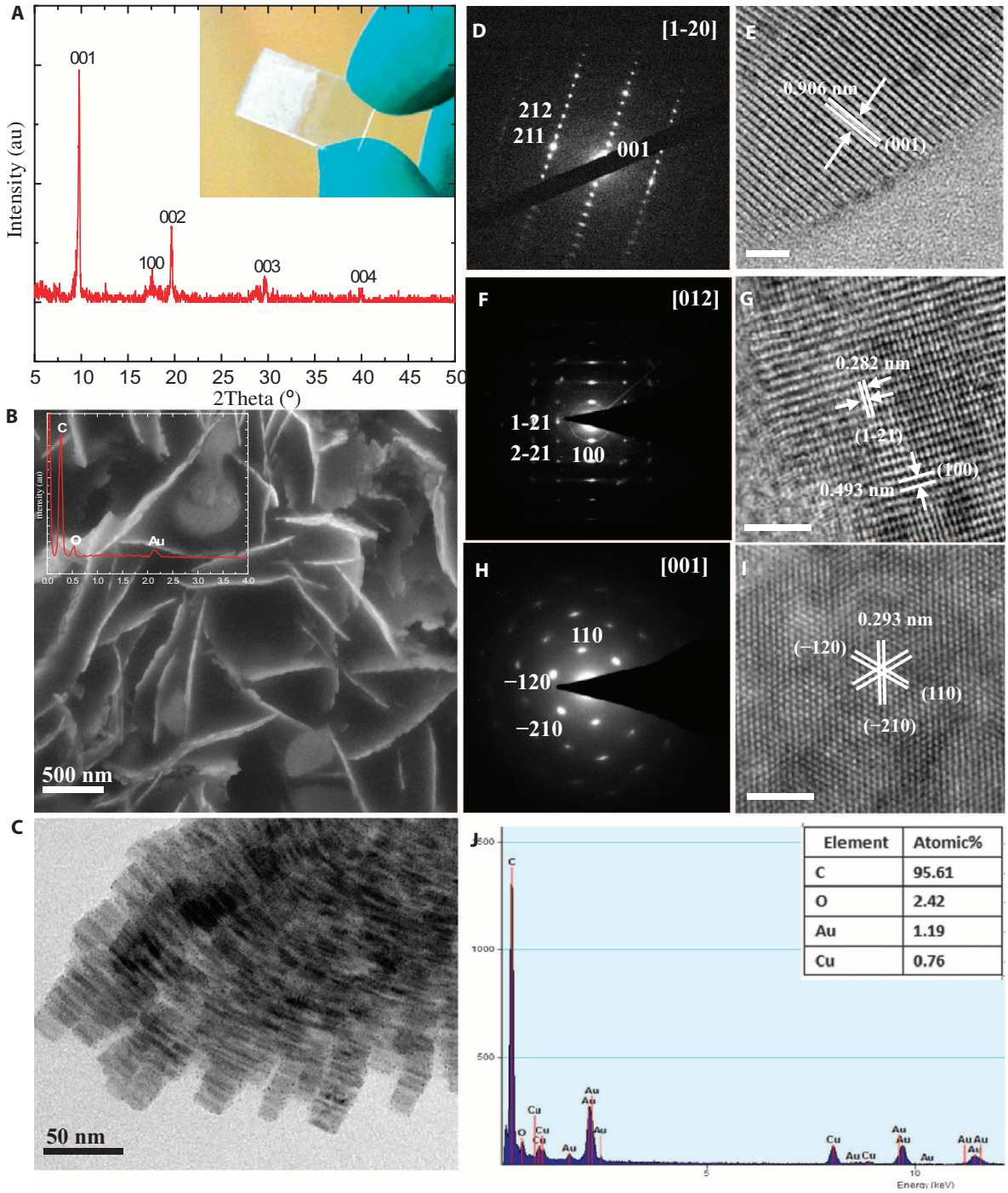

Fig. 4. Morphology and structural characterization of carbyne crystals. (**A**) XRD pattern of the sample. The peaks are shaped and strong, showing the good crystallinity of carbyne. There is an obviously preferred orientation along the *c* axis. Inset: White carbyne powder coating on the glass substrate. Rectangular glass substrate with white crystal powder (left) compared with bare glass (right). (**B**) SEM image of carbyne crystals. They are in the shape of flakes stacked together. EDS showing that the sample contains C, O, and Au. O and Au originate from the surface adsorption of oxygen molecules and gold nanocrystals. (**C**) TEM image of carbyne crystals. Carbyne exhibits a rod shape (10 to 30 nm in width and 50 to >100 nm in length). The tiny spherical particles on the surface of nanorods are gold nanocrystals. (**D** to **I**) SAED patterns and HRTEM images are divided into three categories based on the direction of the incident electron beam ([1-20], [012], and [001], respectively). The former two are rectangular lattices, whereas the last one is a hexagonal lattice. Scale bars, 5 nm (E), 3 nm (G), and 3 nm (H). (**J**) EDS shows that the sample is almost completely composed of carbon and that the Cu signal originated from the Cu grid.

chain, which contains only a single atom in its cross section) should be much easier to bend than a carbon nanotube. These results therefore indicate that a carbyne crystal with a bent structure may be an important characteristic of *sp*-carbon chains. The lengths of the carbon-carbon single bonds and triple bonds in the optimized structure change to 1.27 and 1.30 Å, respectively; this verifies our proposal that bending of the carbyne chains causes variations in bond lengths. We compared the stability of stable carbyne crystals with those of diamond and graphite (Table 1). The carbyne crystal has the highest binding energy among these carbon allotropes, which means that it is a metastable carbon phase. Although they show a metastable property, the carbyne solution and the carbyne crystals remain stable after 6 months of storage (fig. S8). However, carbyne exhibits thermal instability. It transforms into amorphous carbon when temperature is elevated to about 300°C for 30 min (fig. S9).

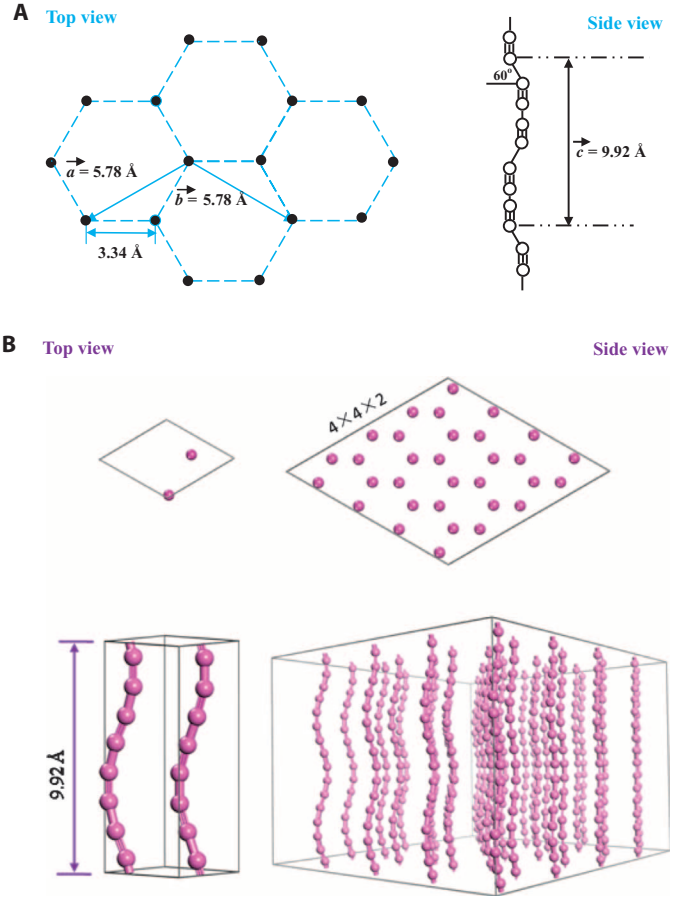

Fig. 5. Carbyne crystal structure. (**A**) The proposed hexagonal structure frame (a = 5.78 Å, b = 5.78 Å, c = 9.92 Å, α = 90°, β = 90°, γ = 120°); the distance between neighboring carbon atoms is 3.34 Å. The corner at the kinks is conjugated by two carbon atoms forming a C–C single bond, and the kinked angle (the angle between the vertical direction and the kinked bond) is 30°. (**B**) The equilibrium configuration of the constructed carbyne crystal based on first-principles calculations. (Left) The unit cell observed from the top (top panel) and side (bottom panel). (Right) The 4 × 4 × 2 supercell observed from the cross-profile perpendicular to the c axis (top panel) and side (bottom panel).

DISCUSSION

To shed light on the mechanism of carbyne formation, we performed thermodynamic and kinetic analyses based on the phase diagram of carbon, the C_2 emission spectrum, and TEM data (Fig. 6). In general, four kinds of chemical reactions take place in laser-induced plasma and at the interface between the liquid and the laser-induced plasma during the transformation of the laser-induced plasma (Fig. 6A), as demonstrated in detail in Supplementary Section I. Carbyne formation is involved in two chemical reactions: the chemical reaction occurring inside the laser-induced plasma wherein reactant species result from the excitation of target and liquid molecules ($T^+ + L^+$) and the chemical reaction occurring at the interface between the laser-induced plasma and the liquid ($T^+ + L$). As shown in Fig. 6B, when alcohol molecules enter the high-temperature and high-pressure plasma region, the hydrogen atom in the hydroxyl group first reacts with active Au ions in the plasma and becomes the Au–H intermediate [reaction (i) in fig. S10]. Sequentially, a pair of α-H and β-H in alcohol molecules is broken under the effect of Au ions as a result of the well-known reaction wherein alcohol is dehydrogenated by gold catalysts (*26*). At the same time, the initial C–C single bonds in alcohol molecules become the C=C double bonds [reaction (ii)]. Afterward, another pair of α-H and β-H breaks again, accompanied by generation of the –C≡C– triple bond connecting with the Au–H intermediates and the oxygen atom. These Au–H intermediates can react with some nucleophiles such as hydroxyl groups or oxygen, which removes hydrogen from the gold surface to generate water (*26*). Finally, the isolated –C≡C– species are synthesized [reaction (iii)]. In our case, these synthesized –C≡C– species are the basic units of the one-dimensional carbyne chain.

In fact, this "–C≡C–" configuration in the final product is similar to a diatomic carbon (or simply a C_2 molecule having the same number of carbon atoms). Recent research showed that the bonding picture of C_2 molecules has been proven to be a major triply bonded structure (*27*), suggesting that C_2 molecules are likely to be the physical entities of the "–C≡C–" configuration in our case. Therefore, we infer that C_2 is the building block of carbyne formation. To check whether C_2 has indeed been generated in the reaction system, we used an in situ spectrum to detect C_2 emission during the laser ablation of the Au target

Table 1. Structure information and binding energy: Carbyne crystal versus graphite and diamond. For comparison, the experimental value of binding energy for graphite is given in brackets.

Structure	Crystal system	Hybridization	Lattice parameters	d_{CC} (Å)	Binding energy (eV/atom)
Carbyne crystal	Hexagonal	*sp*	a = 5.78 Å, b = 5.78 Å, c = 9.92 Å, α = 90°, β = 90°, γ = 120°	1.30, 1.27	−6.347
Graphite	Hexagonal	sp^2	a = 2.46 Å, b = 2.46 Å, c = 6.80 Å, α = 90°, β = 90°, γ = 120°	1.42	−7.844 [−7.41] (*35*)
Diamond	Cubic	sp^3	a = 3.56 Å, b = 3.56 Å, c = 3.56 Å, α = 90°, β = 90°, γ = 90°	1.54	−7.730 [−7.37] (*36*)

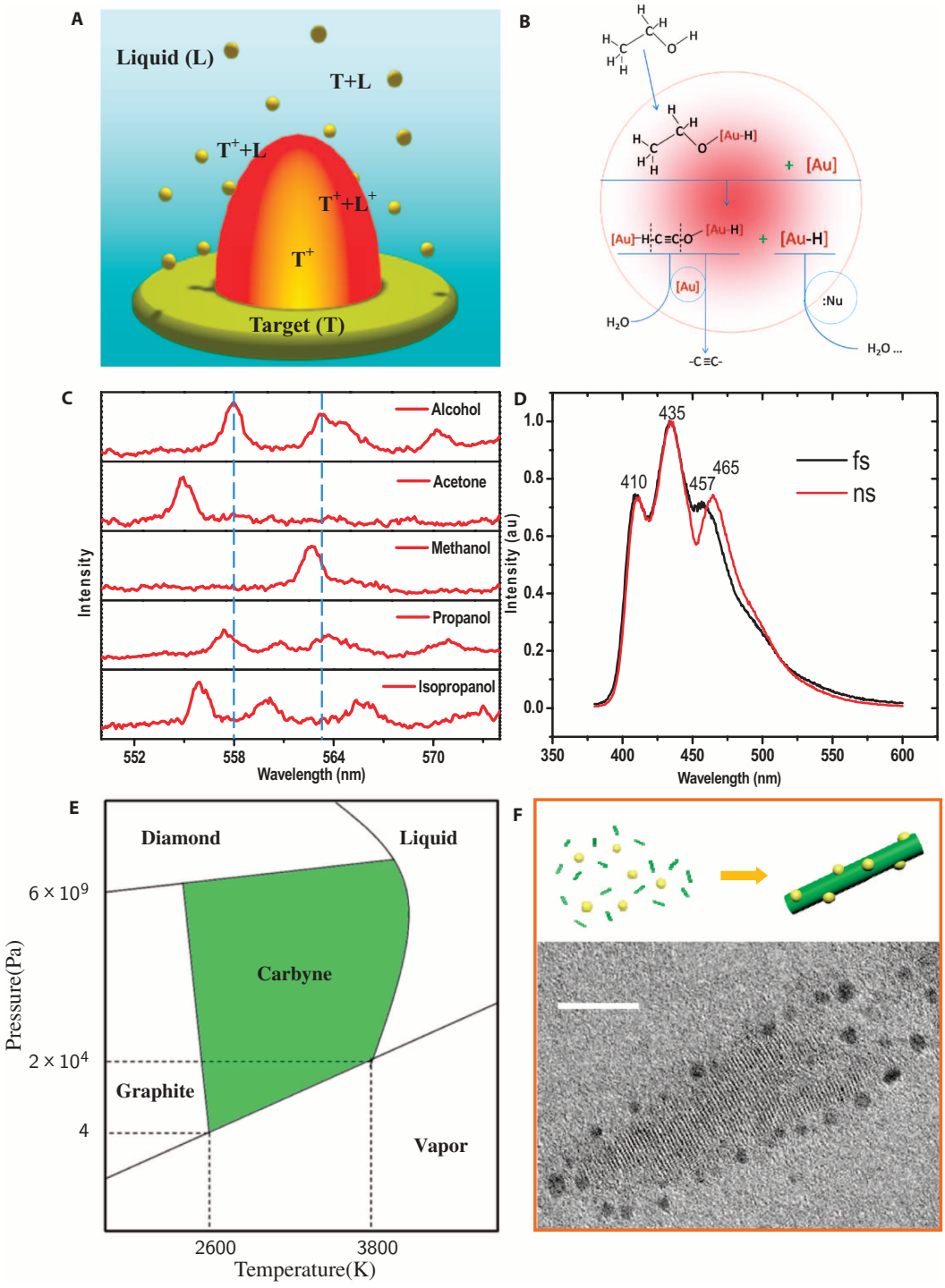

Fig. 6. Mechanism of carbyne formation. (**A**) Schematic illustration of four chemical reactions involved in LAL. Carbyne formation is probably involved in the second kind of chemical reaction occurring inside laser-induced plasma ($T^+ + L^+$) and in the chemical reactions occurring at the interface between the laser-induced plasma and liquid ($T^+ + L$). T^+, laser-induced target plasma; L^+, excited liquid molecules. (**B**) The pathway from alcohol molecules to the carbon-carbon triple bond, in which alcohol dehydrogenated by Au ions plays a key role. [Au], Au ion; :Nu, nucleophile. (**C**) The emission spectra of different solvents during LAL; the peak of alcohol (558.1 and 563.3 nm) in the emission spectrum corresponding to the C_2 swan band for $\Delta v = -1$. The spectra of nonalcohol solvent greatly differ from those of alcohol, and no C_2 signal can be detected. (**D**) Similar fluorescence peaks using nanosecond (ns) and femtosecond (fs) lasers. (**E**) The thermodynamic phase diagram of carbyne adopted by Whittaker (*33*). Green region, the preferred thermodynamic region for carbyne formation. (**F**) Individual carbyne nanorod with gold nanocrystals adheres to its surface; the cartoon depicts how this structure forms. Scale bar, 10 nm.

in alcohol (fig. S11). It turned out that the peaks were located at 558.1 and 563.3 nm in the emission spectrum (Fig. 6C), corresponding to the C_2 swan band for $\Delta v = -1$ (*28*) arising from transitions between the electronic states $d^3\Pi_g$ and $a^3\Pi_u$ (*29*) and providing straightforward evidence for the formation of C_2 molecules in our case. In addition, we collected the spectra of the other kinds of solvent that were similar to alcohol, including methanol, acetone, *n*-propanol, and isopropanol (Fig. 6C). Although these solvents have similar functional groups such as hydroxyl groups, their spectra greatly differs from that of alcohol, and no C_2 signal can be detected. TEM images of the product synthesized from a nonalcohol solvent (figs. S12, A to D, and S13) and a Raman signal (fig. S14) further confirm our results. No carbyne crystals, except for tiny Au nanoparticles, could be observed.

The experimental evidence mentioned above shows that alcohol plays an essential role in the nucleation and growth of carbynes in LAL. In terms of molecular structure, alcohol has two carbon atoms and a hydroxyl group. This configuration with two carbon atoms happens to match that of a diatomic carbon (that is, C_2 molecules). In this way, it is easy to understand why methanol, propanol, and isopropanol cannot form carbyne. Additionally, the hydroxyl in alcohol is also important because the first step in the entire process is the formation of the Au–H intermediate by Au ions reacting with hydroxyl in alcohol. Therefore, we deduce that the solvent in LAL consists of two carbon atoms in a pair and at least one hydroxyl. Under this consideration, alcohol seems to be the best choice for synthesizing carbyne in our case.

Not only did the solvent matter, but the target materials were also key factors in the entire process because they acted as catalysts in the series of chemical reactions mentioned above. We chose platinum as the target material to replace gold. Although platinum has a catalytic property similar to that of Au, no carbyne (based on TEM observations) was found, and only tiny platinum nanoparticles (~2 nm) appeared (fig. S12E). In our case, gold was superior to platinum because the gold surface was preponderantly covered by adsorbed hydrogen (*30*), which may have caused the cleavage of carbon-hydrogen bonds to proceed more readily.

As mentioned above, plasma is involved in a high-temperature and high-pressure state. In our case, temperature was deduced to range from 2500 to 5000 K (*31*), and pressure was deduced to range from 2 to 5 GPa (*32*). The carbyne phase diagram reported by Whittaker (*33*) suggests that carbyne formation is in favor of the high-temperature range of 2600 to 3800 K and the pressure range of 4 to 6 GPa (Fig. 6E). We can clearly see that the thermodynamic environment provided by LAL is very suitable for the nucleation and growth of carbyne and is the stable phase region of carbyne. Therefore, those –C≡C– species from the series of chemical reactions above can easily nucleate and grow in the thermodynamic environment created by LAL. Finally, the carbyne chain forms during plasma quenching.

An "energy threshold" exists based on our experiments. This means that carbyne formation can be achieved only beyond the laser energy threshold under the same focal conditions. In our case, this energy threshold is about 200 mJ/pulse. When laser power is reduced to below 200 mJ/pulse, carbyne becomes difficult to synthesize. This phenomenon can be explained by the fact that the temperature and pressure of the plasma created by LAL strongly depend on laser power (*18*). If laser power is reduced to below the critical value, the temperature and pressure of the plasma will drop correspondingly and thus may not reach the criteria for carbyne formation.

Laser pulse width accounts for much of the size of the final product during LAL. In general, the shorter the laser pulse width is, the shorter the quench time of the plasma is and the smaller the product is (*18*). Therefore, to check whether the laser pulse width can be used to adjust the number of carbon atoms in the synthesized carbyne in our case, we used a femtosecond pulsed laser (35 fs, 4 mJ/pulse, 1000 Hz) instead of a nanosecond laser to perform the same experiment. We successfully synthesized carbyne using femtosecond LAL (fig. S15A). However, the synthesized carbyne still maintains about 10 carbon atoms (fig. S15B and Fig. 6D). Thus, these results show that the formation of a carbyne chain with about 10 carbon atoms by LAL is preferable and that pulse width seems to have no effect on the chain length of carbyne.

The discussion above shows that gold ions in plasma play an essential role in cleaving carbon-hydrogen bonds and in providing sufficiently high temperatures and pressure for carbyne nucleation and growth. Nearby gold nanoparticles closely adhere to the surfaces of carbyne crystals when synthesized carbynes condense into carbyne crystals. Convincingly, the HRTEM image (Fig. 6F) shows that many tiny gold nanoparticles surround individual carbyne crystals. The interplanar spacing of nanoparticles is 0.235 nm, corresponding to the (111) plane of gold. In addition, larger carbyne crystals can be formed by arranging these carbyne nanorods side by side (fig. S16). These Au nanoparticles mostly adhered to carbyne crystals instead of dispersed Au nanoparticles in the carbon grid based on TEM observation, suggesting that there exists some attraction between Au nanoparticles and carbyne crystals. Thus, these results suggest that Au behaves as a soft Lewis acid or electrophile (*34*), whereas the "–C≡C–" triple bond behaves as a nucleophile. These two reagents may lead to an attractive interaction. These Au nanoparticles are inclined to adsorb on the surface of carbyne crystals.

In summary, we obtained sufficient solid experimental evidence to substantiate the synthesis of carbyne with finite length under ambient conditions in the laboratory using LAL. We also showed strong purple-blue fluorescence from the intrinsic emissions of carbyne. We produced hexagonal carbyne crystals (that is, the condensed phase of carbyne) through the natural drying of a solution of synthesized carbyne, and theoretical calculations confirmed that the carbyne crystal is a metastable phase of carbon. This method is suitable for carbyne synthesis, enabling the exploration of the properties and potential applications of carbyne.

MATERIALS AND METHODS

Carbyne synthesis

Carbyne synthesis was performed using LAL (*17*). A gold target (99.99% purity) was fixed on the bottom of a quartz chamber. Absolute ethanol was poured into the chamber until the target was covered by 8 mm. The second harmonic produced by a Q-switched Nd:YAG laser device (with a wavelength of 532 nm, a pulse width of 10 ns, a repetition frequency of 5 Hz, and a laser pulse energy of 500 mJ) was focused on the target. The spot size was smaller than 1 mm. A continuous nitrogen flow prevented the alcohol from burning. After 30 min, the solution was analyzed using HPLC. The samples obtained at 2.3 min were collected for characterization. Carbyne is soluble in organic solvents (such as alcohol, acetone, and toluene) but is insoluble in water. We estimate solubility as follows: 2 ml of alcohol can dissolve 0.1 mg of carbyne; therefore, solubility was estimated to be higher than that (0.05 mg/ml) of alcohol. Because the scale of the sample in one synthesis was limited, we accumulated the sample for about 10 syntheses. The scale of the sample was 0.987 mg. After HPLC treatment, the scale of the sample was reduced to 0.102 mg.

Carbyne characterization

HPLC was used to separate specimens from the as-synthesized solution. The solution was filtered through a column (Zorbax Eclipse XDB-C8) in a high-performance liquid chromatograph (series 1200; Agilent Technologies), with methanol/water (97:3, v/v) as mobile phase. The carbynes eluted from the column were identified using a diode array detector. The Raman and FTIR spectra of the samples deposited on silicon substrates were recorded using a Renishaw inVia Plus Laser micro-Raman spectrometer (with laser irradiation at λ = 514 and 633 nm) and a Bruker Equinox 55 spectrometer coupled with an infrared microscope, respectively. UV-Vis spectra of the samples were obtained using a UV 3150 spectrophotometer (Shimadzu). Fluorescence measurements were performed at room temperature using an Edinburgh FLS920 spectrofluorophotometer with a 450-W xenon lamp and a photomultiplier tube operated in photon-counting mode as detector. The gas chromatography–mass spectrometry (GC-MS) data of carbyne were recorded with a Finnigan Voyager GC-8000 Top Series GC-MS System with an electron impact mass selective detector. The following oven temperature program was adopted: the temperature was kept at 40°C for 2 min, increased by 5°C/min up to 110°C, and increased by 15°C/min up to 250°C, which was kept constant for a further 2 min. The carbyne solution was dried at room temperature, and the sample was dissolved again in methanol-d_4 for ^{13}C NMR (500 MHz, Bruker Avance III).

Characterization of carbyne crystals

XRD was performed using a Rigaku D/Max-IIIA x-ray diffractometer with Cu Kα radiation (λ = 1.54056 Å, 40 kV, 20 mA) at a scanning rate of 2 deg/s. TEM images, SAED patterns, and HRTEM images were obtained using a JEOL JEM-2010HR instrument (at an accelerating voltage of 200 kV), an FEI Tecnai G2 F30 transition electron microscope equipped with a field emission gun (at an accelerating voltage of 300 kV), and an EDX spectrometer. The sample was pipetted onto a carbon support film on a copper grid. SEM images of the as-synthesized samples were obtained using a Quanta 400F field emission scanning electron microscope operated at 10 kV.

Theoretical calculations

The theoretical calculations were divided into four parts: determination of the electronic properties of the linear carbyne, simulation of the Raman spectrum of carbyne, evaluation of the stability of carbyne, and determination of the structure and stability of carbyne crystals. The details of all calculation processes are available in the Supplementary Materials.

SUPPLEMENTARY MATERIALS

Supplementary material for this article is available at http://advances.sciencemag.org/cgi/content/full/1/9/e1500857/DC1

REFERENCES AND NOTES

1. H. W. Kroto, J. R. Heath, S. C. O'Brien, R. F. Curl, R. E. Smalley, C_{60}: Buckminsterfullerene. *Nature* **318**, 162–163 (1985).
2. E. H. L. Falcao, F. Wudl, Carbon allotropes: Beyond graphite and diamond. *J. Chem. Technol. Biotechnol.* **82**, 524–531 (2007).
3. H. O. Pierson, *Handbook of Carbon, Graphite, Diamond and Fullerenes—Properties, Processing and Applications* (William Andrew/Noyes, Norwich, NY, 1993).
4. S. Iijima, Helical microtubules of graphitic carbon. *Nature* **354**, 56–58 (1991).
5. C. Frondel, U. B. Marvin, Lonsdaleite, a hexagonal polymorph of diamond. *Nature* **214**, 587–589 (1967).
6. P. Liu, H. Cui, G. W. Yang, Synthesis of body-centered cubic carbon nanocrystals. *Cryst. Growth Des.* **8**, 581–586 (2008).
7. M. M. Haley, Carbon allotropes: On the road to carbyne. *Nat. Chem.* **2**, 912–913 (2010).
8. W. A. Chalifoux, R. R. Tykwinski, Synthesis of polyynes to model the *sp*-carbon allotrope carbyne. *Nat. Chem.* **2**, 967–971 (2010).
9. A. G. Whittaker, E. J. Watts, R. S. Lewis, E. Anders, Carbynes: Carriers of primordial noble gases in meteorites, *Science* **209**, 1512–1514 (1980).
10. A. El Goresy, G. Donnay, A new allotropic form of carbon from the Ries Crater. *Science* **161**, 363–364 (1968).
11. A. G. Whittaker, P. L. Kintner, Carbon: Observations on the new allotropic form. *Science* **165**, 589–591 (1969).
12. V. V. Korshak, Y. P. Kudryavtsev, V. V. Khvostov, M. B. Guseva, V. G. Babaev, O. Y. Rylova, Electronic structure of carbynes studied by Auger and electron energy loss spectroscopy. *Carbon* **25**, 735–738 (1987).
13. R. J. Lagow, J. J. Kampa, H.-C. Wei, S. L. Battle, J. W. Genge, D. A. Laude, C. J. Harper, R. Bau, R. C. Stevens, J. F. Haw, E. Munson, Synthesis of linear acetylenic carbon: The "*sp*" carbon allotrope. *Science* **267**, 362–367 (1995).
14. W. A. Chalifoux, R. R. Tykwinski, Synthesis of extended polyynes: Toward carbyne. *C. R. Chim.* **12**, 341–358 (2009).
15. R. B. Heimann, J. Kleiman, N. M. Salansky, A unified structural approach to linear carbon polytypes. *Nature* **306**, 164–167 (1983).
16. H. Kroto, Carbyne and other myths about carbon. *Chem. World* **7**, 37 (2010).
17. P. P. K. Smith, P. R. Buseck, Carbyne forms of carbon: Do they exist? *Science* **216**, 984–986 (1982).
18. G. W. Yang, Laser ablation in liquids: Applications in the synthesis of nanocrystals. *Prog. Mater. Sci.* **52**, 648–698 (2007).
19. L. K. Robert, B. Heimann, Sergey E. Evsyukov, *Carbyne and Carbynoid Structures* (Kluwer, Dordrecht, Netherlands, 1999).
20. L. Ravagnan, F. Siviero, C. Lenardi, P. Piseri, E. Barborini, P. Milani, C. S. Casari, A. Li Bassi, C. E. Bottani, Cluster-beam deposition and in situ characterization of carbyne-rich carbon films. *Phys. Rev. Lett.* **89**, 285506 (2002).
21. E. Mullazzi, G. P. Brivio, E. Faulques, S. Lefrant, Experimental and theoretical Raman results in trans polyacetylene. *Solid State Commun.* **46**, 851–855 (1983).
22. T. Gibtner, F. Hampel, J.-P. Gisselbrecht, A. Hirsch, End-cap stabilized oligoynes: Model compounds for the linear sp carbon allotrope carbyne. *Chem. Eur. J.* **8**, 408–432 (2002).
23. F. Cataldo, Polyynes: A new class of carbon allotropes. About the formation of dicyanopolyynes from an electric arc between graphite electrodes in liquid nitrogen. *Polyhedron* **23**, 1889–1896 (2004).
24. Y. H. Hu, Bending effect of sp-hybridized carbon (carbyne) chains on their structures and properties. *J. Phys. Chem. C* **115**, 1843–1850 (2011).
25. P. Ordejón, E. Artacho, J. M. Soler, Self-consistent order-*N* density-functional calculations for very large systems. *Phys. Rev. B Condens. Matter* **53**, R10441–R10444 (1996).
26. M. Conte, H. Miyamura, S. Kobayashi, V. Chechik, Spin trapping of Au–H intermediate in the alcohol oxidation by supported and unsupported gold catalysts. *J. Am. Chem. Soc.* **131**, 7189–7196 (2009).
27. P. Su, J. Wu, J. Gu, W. Wu, S. Shaik, P. C. Hiberty, Bonding conundrums in the C_2 molecule: A valence bond study. *J. Chem. Theory Comput.* **7**, 121–130 (2011).
28. J. Xiao, P. Liu, G. W. Yang, Nanodiamonds from coal under ambient conditions. *Nanoscale* **7**, 6114–6125 (2015).

29. P. S. Shell, L. M. Jackman, S. Ahmed, M. L. McKee, P. B. Shenlin, Some reactions and properties of molecular C_2. An experimental and theoretical treatment. *J. Am. Chem. Soc.* **111**, 4422–4429 (1989).
30. J. Schwank, Catalytic gold. *Gold Bull.* **16**, 103–110 (1983).
31. T. Sakka, H. Oguchi, Y. H. Ogata, Emission spectroscopy of ablation plumes in liquid for analytical purposes. *J. Phys. Conf. Ser.* **59**, 559–562 (2007).
32. L. Berthe, A. Sollier, P. Peyere, R. Fabbro, E. Bartnicki, The generation of laser shock waves in a water-confinement regime with 50 ns and 150 ns XeCl excimer laser pulses. *J. Phys. D Appl. Phys.* **33**, 2142 (2000).
33. A. G. Whittaker, Carbon: A new view of its high-temperature behavior. *Science* **200**, 763–764 (1978).
34. R. Skouta, C.-J. Li, Gold-catalyzed reactions of C–H bonds. *Tetrahedron* **64**, 4917–4938 (2008).
35. N. N. Greenwood, A. Earnshaw, *Chemistry of the Elements* (Pergamon, Oxford, UK, 1984).
36. S. Fahy, X. W. Wang, S. G. Louie, Variational quantum Monte Carlo nonlocal pseudopotential approach to solids: Cohesive and structural properties of diamond. *Phys. Rev. Lett.* **61**, 1631–1634 (1988).
37. J. M. Soler, E. Artacho, J. D. Gale, A. Garcia, J. Junquera, P. Ordejón, D. Sánchez-Portal, The SIESTA method for ab initio order-*N* materials simulation. *J. Phys. Condens. Matter* **14**, 2745 (2002).
38. N. Troullier, J. L. Martins, Efficient pseudopotentials for plane-wave calculations. *Phys. Rev. B Condens. Matter* **43**, 1993–2006 (1991).
39. J. P. Perdew, K. Burke, M. Ernzerhof, Generalized gradient approximation made simple. *Phys. Rev. Lett.* **77**, 3865–3868 (1996).
40. S. J. Clark, M. D. Segall, C. J. Pickard, P. J. Hasnip, M. I. J. Probert, K. Refson, M. C. Payne, First principles methods using CASTEP. *Z. Kristallogr.* **220**, 567–570 (2005).
41. L. D. Field, S. Sternhell, J. R. Kalman, *Organic Structures from Spectra* (John Wiley & Sons Ltd., New York, ed. 3, 2002).
42. J. C. Dobrowolski, A. P. Mazurek, The granny and square carbyne knots: Theoretical NMR spectra. *J. Mol. Struct.* **482**, 339–342 (1999).

Funding: We acknowledge the National Basic Research Program of China (2014CB931700), the National Natural Science Foundation of China (91233203), and the State Key Laboratory of Optoelectronic Materials and Technologies for supporting this work. **Author contributions:** B.P., J.X., and J.L. performed experimental and theoretical work. P.L. and C.W. performed data analysis. G.Y. planned the project. **Competing interests:** The authors declare that they have no competing interests. **Data and materials availability:** All data needed to evaluate the conclusions in the paper are present in the paper and/or the Supplementary Materials. Additional data related to this paper will be made available by the authors upon request.

Submitted 28 June 2015
Accepted 31 August 2015
Published 30 October 2015
10.1126/sciadv.1500857

Citation: B. Pan, J. Xiao, J. Li, P. Liu, C. Wang, G. Yang, Carbyne with finite length: The one-dimensional *sp* carbon. *Sci. Adv.* **1**, e1500857 (2015).